Available online at www.sciencedirect.com
SCIENCE DIRECT
Journal of Solid State Chemistry 179 (2006) 1434–1444
JOURNAL OF SOLID STATE CHEMISTRY
www.elsevier.com/locate/jssc

Synthesis and characterization of $Sr_{0.75}Y_{0.25}Co_{1-x}M_xO_{2.625+\delta}$ (M = Ga, $0.125 \leqslant x \leqslant 0.500$ and M = Fe, $0.125 \leqslant x \leqslant 0.875$)

F. Lindberg[a], O.A. Drozhzhin[b], S.Ya. Istomin[c,*], G. Svensson[a], F.B. Kaynak[d], P. Svedlindh[e], P. Warnicke[e], A. Wannberg[f], A. Mellergård[f], E.V. Antipov[c]

[a]Department of Structural Chemistry, Stockholm University, SE-106 91 Stockholm, Sweden
[b]Department of Materials Science, Moscow State University, 119992 Moscow, Russia
[c]Department of Chemistry, Moscow State University, 119992 Moscow, Russia
[d]Department of Physics Engineering, Faculty of Engineering, Hacettepe University, 06800, Ankara, Turkey
[e]Department of Engineering Sciences, Uppsala University, Box 534, SE-751 21, Uppsala, Sweden
[f]Studsvik Neutron Research Laboratory, Uppsala University, SE-611 82 Nyköping Sweden

Received 9 November 2005; received in revised form 27 January 2006; accepted 28 January 2006
Available online 3 March 2006

Abstract

The effect of replacing Co^{3+} by Ga^{3+} and Fe^{3+} in the perovskite-related tetragonal phase $Sr_{0.75}Y_{0.25}CoO_{2.625}$ with unit cell parameters: $a = 2a_p$, and $c = 4a_p$ (314 phase) has been investigated. The 314 phase is formed by $Sr_{0.75}Y_{0.25}Co_{1-x}M_xO_{2.625+\delta}$, with $x \leqslant 0.375$ for M = Ga and $x \leqslant 0.625$ for M = Fe. High-resolution transmission electron microscopy and electron diffraction revealed frequent microtwinning in the iron-containing compounds, in contrast to the Ga-substituted 314 phases. Diffraction experiments and electron microscope images indicated that at higher Fe contents, $0.75 \leqslant x \leqslant 0.875$, a disordered cubic perovskite structure forms. The crystal structures of $Sr_{0.75}Y_{0.25}Co_{0.75}Ga_{0.25}O_{2.625}$ and $Sr_{0.75}Y_{0.25}Co_{0.5}Fe_{0.5}O_{2.625+\delta}$ were refined using neutron powder diffraction data. It was found that the oxygen content of $Sr_{0.75}Y_{0.25}Co_{0.5}Fe_{0.5}O_{2.625+\delta}$ is higher than in Fe-free 314 phase, so that δ corresponds to 0.076, whereas $\delta = 0$ in $Sr_{0.75}Y_{0.25}Co_{0.75}Ga_{0.25}O_{2.625+\delta}$. Magnetization measurements on the unsubstituted $Sr_{0.7}Y_{0.3}CoO_{2.62}$ and Ga-substituted $Sr_{0.75}Y_{0.25}Co_{0.75}Ga_{0.25}O_{2.625}$ compounds indicate the presence of a ferromagnetic-like contribution to the measured magnetization at 320 and 225 K, respectively, while replacing Co by Fe leads to the suppression of this contribution. A neutron diffraction study shows that the $Sr_{0.75}Y_{0.25}Co_{0.5}Fe_{0.5}O_{2.625+\delta}$ compound is G-type antiferromagnetic at room temperature, whereas $Sr_{0.75}Y_{0.25}Co_{0.75}Ga_{0.25}O_{2.625}$ does not exhibit magnetic ordering at room temperature.

Keywords: 314 phases; Neutron diffraction; Electron diffraction; Crystal structure

1. Introduction

The ease of forming ordered oxygen vacancies makes the family of oxygen-deficient perovskite-related compounds ABO_{3-y} very comprehensive. For some systems, the oxidation state of the B cation can easily be varied so that a number of oxygen-deficient compounds can be isolated. The A cation is in most cases an alkali, alkaline-earth or a rare-earth cation and can thus not easily be oxidized or reduced. Instead, heterovalent substitution of the A cation can be used to prepare oxygen-deficient perovskites. Some of us have shown in previous articles the effects of doping with lanthanides and yttrium in the $Sr_{1-x}Ln_xCoO_{3-y}$ system [1,2] (hereafter referred to as 314 phase). It was established that the compounds $Sr_{0.7}Ln_{0.3}CoO_{2.62}$ (Ln = Y, Eu–Ho) crystallize with a tetragonal perovskite-related superstructure (space group $I4/mmm$, $a \approx 2a_p$ and $c \approx 4a_p$) [2], see Fig. 1a. The structure of the 314 phase has some similarities to brownmillerite ($Ca_2(Fe,Al)_2O_5$) [3], shown in Fig. 1b, for it consists of alternating layers of tetrahedra and octahedra. However, due to ordering of Sr^{2+} and Ln^{3+} in the $Sr_{0.7}Ln_{0.3}CoO_{2.62}$ structure, the tetrahedra form tetracyclic Co_4O_{12} units instead of the infinite chains

*Corresponding author. Fax: +7 095 939 47 88.
E-mail address: istomin@icr.chem.msu.ru (S.Y. Istomin).

0022-4596/$ - see front matter © 2006 Elsevier Inc. All rights reserved.
doi:10.1016/j.jssc.2006.01.057

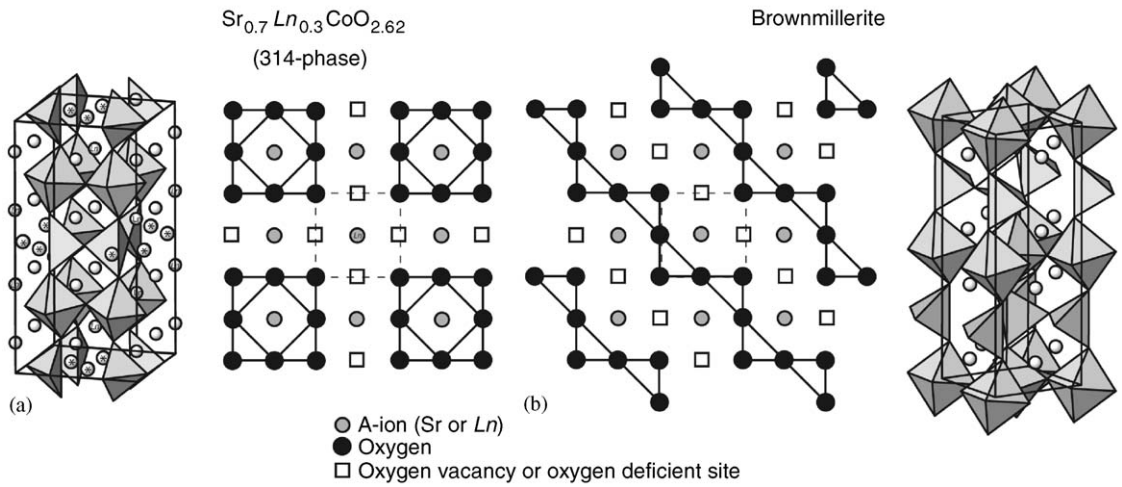

Fig. 1. Crystal structure of $Sr_{0.7}Y_{0.3}CoO_{2.62}$ (a) and brownmillerite (b). The drawing in between illustrates a section through the layers of tetrahedra. It is believed that the formation of tetracyclic Co_4O_{12} units in the $Sr_{0.7}Y_{0.3}CoO_{2.62}$ structure type is due to ordering of the *A* cations.

of tetrahedra found in the brownmillerite structure, see Fig. 1. Furthermore, as the chemical formula implies, there are extra oxygen atoms accommodated in the structure of $Sr_{0.7}Y_{0.3}CoO_{2.62}$ compared to brownmillerites. These extra oxygen atoms are randomly located at fourfold split positions in the layers of tetrahedra, so that five-coordinated cobalt atoms are locally present in the structure. The stability range of $Sr_{1-x}Ln_xCoO_{3-y}$ varies with the size of *Ln*; $x = 0.3-0.4$ for Eu, 0.3–0.5 for Gd, 0.3–0.4 for Tb, 0.2–0.3 for Dy, 0.3 for Ho and Y [2].

Cobalt-based perovskite-related oxides with Co^{3+} are known to have interesting magnetic properties like anti-ferromagnetism (AFM), ferromagnetism (FM) and spin clustering. Moreover, due to the small energy differences between the spin states of Co^{3+} (LS, HS or IS) [4], subtle structure changes can promote transformations between these spin states, resulting in a variation of the type of magnetic ordering. Neutron diffraction studies of $Sr_{1-x}Ln_xCoO_{3-\delta}$ with the 314 structure showed their magnetic structures to be G-type antiferromagnetic [2]. However, a detailed study of $Sr_{2/3}Y_{1/3}CoO_{8/3+\delta}$, made by Maignan et al. [5], revealed that only a minor insertion of extra oxygen ($\delta = 0.04$), leads to collapse of the orbital ordering present in the unoxidized compound and to a transition from an AFM to a FM state. Moreover, the change was accompanied by a metal–insulator transition.

It is of interest to establish how replacement of cobalt in the 314 phase by other different *B* cations can influence the crystal structure and magnetic properties. In the present paper we report on the preparation, the crystal and magnetic structures and magnetic properties of the gallium and iron substituted Y-314 phase $Sr_{0.75}Y_{0.25}Co_{1-x}M_xO_{2.625+\delta}$ (M = Ga, $0.125 \leqslant x \leqslant 0.500$ and M = Fe, $0.125 \leqslant x \leqslant 0.875$).

2. Experimental

$Sr_{0.75}Y_{0.25}Co_{1-x}M_xO_{2.625+\delta}$, M = Fe, $x = 0.125-1.0$; M = Ga; $x = 0.125-0.5$, $\Delta x = 0.125$ for both, were synthesized by the citrate method. Stoichiometric amounts of $SrCO_3$, Y_2O_3, $FeC_{15}H_{21}O_6$, $Ga(NO_3)_3 \cdot 8H_2O$ and $Co(NO_3)_3 \cdot 6H_2O$ (all of 99% purity or higher) were dissolved in a melt of citric acid. The mixture was heated to decomposition and then fired in air at 650 °C for 12 h, followed by grinding, pellet pressing of the powders, and sintering in air at 1100 °C for 24 h. The purity of the compounds was checked by means of their X-ray powder diffraction (XRD) photographs recorded with a Guinier–Hägg camera with Cu$K\alpha_1$ radiation, using Si or Ge as internal standard. Neutron powder diffraction (NPD) data were collected at the Swedish research reactor at NFL, Studsvik, using the R2D2 diffractometer equipped with ^{3}He detectors and a Ge (511) monochromator, $\lambda = 1.551$ Å, between $2\theta = 4°$ and 140°. A thin vanadium can with diameter 6 mm was used as a sample holder. For the structure refinements based on the NPD data the GSAS suite of programs [6] was used. The scattering lengths of the different atoms were taken from the program library.

Transmission electron microscopy (TEM) studies were done on small amounts of the samples, which had been dispersed in butanol and put on a holey carbon film supported by a copper grid. The microscopes used were JEOL JEM3010 UHR, operated at 300 kV for high-resolution (HRTEM) studies, and JEOL JEM2000FX, 200 kV equipped with a LINK AN10000 energy-dispersive X-ray microanalysis (EDX) system for elemental analysis and electron diffraction (ED).

The magnetic measurements were performed in a Quantum Design MPMS-XL Superconducting Quantum Interference Device (SQUID) magnetometer. Magnetization versus temperature was studied between 5 and 400 K, following two different protocols: zero field cooled (ZFC) and field cooled (FC) on $Sr_{0.75}Y_{0.25}Co_{0.75}Ga_{0.25}O_{2.625+\delta}$ and $Sr_{0.75}Y_{0.25}Co_{0.5}Fe_{0.5}O_{2.625+\delta}$ samples, and for comparison also on $Sr_{0.7}Y_{0.3}CoO_{2.62}$. The ZFC magnetization was obtained by cooling the sample to 5 K in zero field, turning on a magnetic field of 20 Oe and measuring the

Table 1
Unit cell parameters and c/a ratio for $Sr_{0.75}Y_{0.25}Co_{1-x}Fe_xO_{2.625+\delta}$ ($0.0 \leqslant x \leqslant 0.875$) and $Sr_{0.75}Y_{0.25}Co_{1-x}Ga_xO_{2.625}$ ($0.0 \leqslant x \leqslant 0.375$), values for $Sr_{0.7}Y_{0.3}CoO_{2.62}$ are taken from [1] and put in row $x = 0$

X	$Sr_{0.75}Y_{0.25}Co_{1-x}Ga_xO_{2.625}$			$Sr_{0.75}Y_{0.25}Co_{1-x}Fe_xO_{2.625+\delta}$		
	a	c	c/a	a	c	c/a
0	7.6237(8)	15.314(2)	2.009	7.6237(8)	15.314(2)	2.009
0.125	7.660(1)	15.290(5)	1.996	7.640(2)	15.339(6)	2.008
0.250	7.674(2)	15.311(5)	1.995	7.659(2)	15.334(6)	2.002
0.375	7.686(1)	15.318(5)	1.993	7.670(3)	15.345(3)	2.001
0.500				7.687(1)	15.364(1)	1.999
0.625				3.8513(6)		
0.750				3.8556(3)		
0.875				3.8610(5)		

magnetization as the sample warmed up to 400 K. The FC magnetization was subsequently obtained by measuring the magnetization, in the same applied field, as the sample cooled down to 5 K. Isothermal magnetization measurements were performed at 10, 120 and 280 K, by applying a large positive magnetic field (20 or 50 kOe) and measuring the magnetization as a function of decreasing field. Since the experimental results indicate a spin-canted antiferromagnetic behaviour, the field sweep was continued to negative fields until the magnetization changed sign.

3. Results

The products formed after heat treatment were black powders. XRD single-phase samples were prepared of $Sr_{0.75}Y_{0.25}Co_{1-x}Ga_xO_{2.625+\delta}$, $x \leqslant 0.375$. All the compounds are isostructural with the Y-314 phase. For $x > 0.375$, additional reflections from CoO, Y_2O_3 and $Sr_3Ga_4O_9$ appeared in the XRD patterns, besides those from the 314 phase.

Single-phase samples were prepared of $Sr_{0.75}Y_{0.25}Co_{1-x}Fe_xO_{2.625+\delta}$ for $x \leqslant 0.875$. XRD patterns of $Sr_{0.75}Y_{0.25}Co_{1-x}Fe_xO_{2.625+\delta}$, Fe $x \leqslant 0.5$, were indexed with tetragonal unit cells; the parameters (Table 1) indicating them to be isostructural with the 314 phase. No splitting of the perovskite subcell reflections, and appearance of superstructure reflections were observed in the XRD pattern of $Sr_{0.75}Y_{0.25}Co_{1-x}Fe_xO_{2.625+\delta}$, $0.625 \leqslant x \leqslant 0.875$. However, a preliminary study of $Sr_{0.75}Y_{0.25}Co_{0.375}Fe_{0.625}O_{2.625+\delta}$ by NPD revealed the presence of superstructure reflections corresponding to the 314 structure. The $Sr_{0.75}Y_{0.25}FeO_{2.625+\delta}$ composition yielded only multiphase samples.

The perovskite subcell volumes versus x for $Sr_{0.75}Y_{0.25}Co_{1-x}M_xO_{2.625+\delta}$, $M = Ga$, $x \leqslant 0.375$ and Fe, $x \leqslant 0.875$ are given in Fig. 2.

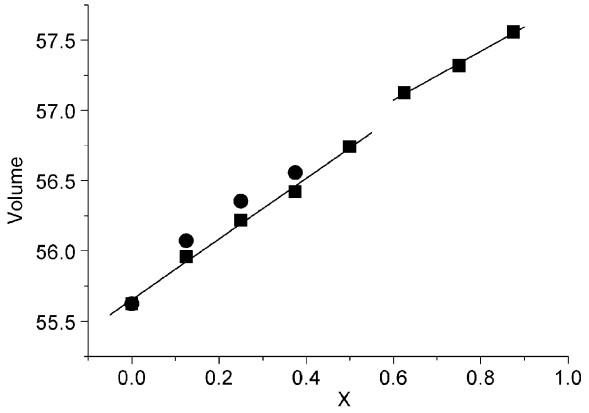

Fig. 2. The volume of the perovskite subcell versus x for $Sr_{0.75}Y_{0.25}Co_{1-x}M_xO_{2.625+\delta}$, $M = Ga$ (circles), Fe (squares). Two linear parts are seen for $M = Fe$, corresponding to the compositions with 314 phase and cubic perovskite structures, respectively.

Table 2
Crystal data and details from the Rietveld refinement of $Sr_{0.75}Y_{0.25}Co_{0.5}Fe_{0.5}O_{2.625+\delta}$ and $Sr_{0.75}Y_{0.25}Co_{0.75}Ga_{0.25}O_{2.625}$

Compound	$Sr_{0.75}Y_{0.25}Co_{0.75}Ga_{0.25}O_{2.625}$	$Sr_{0.75}Y_{0.25}Co_{0.5}Fe_{0.5}O_{2.625+\delta}$
a/Å	7.6547(1)	7.6819(2)
c/Å	15.3542(4)	15.3822(6)
Space-group	$I4/mmm$	$I4/mmm$
Magnetic space-group	—	$I4'/mmm$
χ^2	3.997	3.182
R_{wp}	0.0331	0.0355
R_p	0.0263	0.0289
No. refl.	281	416
R_F^2	0.0358	0.0285
Fitted parameters	54	56

3.1. Neutron powder diffraction study

For the refinement of the $Sr_{0.75}Y_{0.25}Co_{0.75}Ga_{0.25}O_{2.625}$ and $Sr_{0.75}Y_{0.25}Co_{0.5}Fe_{0.5}O_{2.625+\delta}$ crystal structures, initial atomic coordinates were taken from the crystal structure of $Sr_{0.7}Y_{0.3}CoO_{2.62}$ [1]. Crystal data and details of the refinements are presented in Table 2. Observed, calculated and difference NPD patterns for $Sr_{0.75}Y_{0.25}Co_{0.75}Ga_{0.25}O_{2.625}$ and $Sr_{0.75}Y_{0.25}Co_{0.5}Fe_{0.5}O_{2.625+\delta}$ are shown

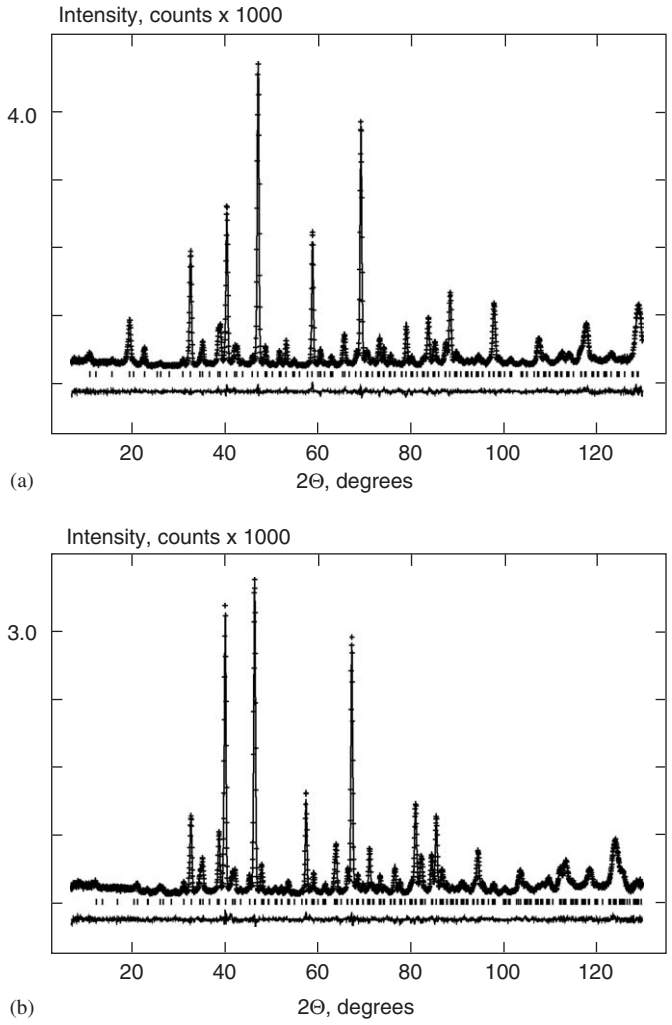

Fig. 3. Observed and calculated neutron diffraction patterns for (a) $Sr_{0.75}Y_{0.25}Co_{0.5}Fe_{0.5}O_{2.625+\delta}$ and (b) $Sr_{0.75}Y_{0.25}Co_{0.75}Ga_{0.25}O_{2.625}$.

in Fig. 3. Final atomic coordinates and atomic displacement parameters are given in Table 3. Some comments on the refinement procedures should be made:

- As expected, it was not possible to determine the preferred positions for Sr and Y, due to the similar scattering lengths: 0.702×10^{-12} and 0.775×10^{-12} cm for Sr and Y, respectively [7] (compare e.g. with 0.945×10^{-12}, 0.249×10^{-12} and 0.729×10^{-12} cm for Fe, Co and Ga, respectively). However, as mentioned above, the Ln^{3+} and Sr^{2+} ions are known to be partially ordered in this type of structure (Ln = Y, Sm–Tm) [2]. Ln^{3+} preferably occupies the 8 + 1 coordinated site 4*e* (0, 0, y). Therefore, this site was assumed to be fully occupied by Y.
- For $Sr_{0.75}Y_{0.25}Co_{0.75}Ga_{0.25}O_{2.625+\delta}$ the Co:Ga ratio was refined to 0.76:0.24(1) and the occupation of the Co:Fe sites to 0.49:0.51(1). These values are in good agreement with nominal compositions and those found from TEM EDX (Co:Ga = 0.75(1):0.25(1) and Co:Fe = 0.48(2):0.52(1)).

Table 3
Atomic coordinates, displacement parameters (× 100) and site occupancies for $Sr_{0.75}Y_{0.25}Co_{0.75}Ga_{0.25}O_{2.625}$ and $Sr_{0.75}Y_{0.25}Co_{0.5}Fe_{0.5}O_{2.625+\delta}$

Atom, site		M = Ga	M = Fe
Sr1, 4*e*; 0, 0, *z*	*z*	0.8764(3)	0.8751(4)
	U_{iso}	2.0(1)	1.7 (1)
Sr2, 8*g*; 0, 0.5, *z*	*z*	0.8666(2)	0.8669(3)
	U_{iso}	1.1(1)	0.91 (8)
Y, 4*e*; 0, 0, *z*	*z*	0.3526(2)	0.3538(3)
	U_{iso}	1.5(1)	2.3 (2)
Co1/*M*1, 8*h*; *x*, *x*, 0	*x*	0.2475(2)	0.2530(3)
	U_{iso}	1.7(1)	1.2 (1)
	Frac	0.63/0.37(1)	0.531/0.469(9)
	M_z	0	−1.82(5)
Co2/*M*2, 8*f*; 0.25, 0.25, 0.25	*x*		
	U_{iso}	0.7(1)	0.8(1)
	Frac	0.892 /0.108(9)	0.450/0.550(9)
	M_z	0	2.58(5)
O1, 16*n*; 0, *y*, *z*	*y*	0.2449(2)	0.2460(3)
	z	0.2397(1)	0.2389(2)
	U_{iso}	0.73(3)	0.76(6)
O2, 16*m*; *x*, *x*, *z*	*x*	0.2874(2)	0.2858(3)
	z	0.1162(1)	0.1186(2)
	U_{iso}	2.51(7)	2.8(1)
O3, 8*i*; 0, *x*, 0	*x*	0.7213(5)	0.7200(7)
	U_{iso}	2.16(8)	1.7(1)
O4, 8*j*; *x*, 0.5, 0	*x*	0.389(1)	0.400(2)
	Frac	0.25(1)	0.249(8)
	U_{iso}	1.8(2)	2.0[a]
O5, 8*j*; *x*, 0.5, 0.0	*x*	—	0.237(4)
	Frac		0.151(8)
	U_{iso}		2.0[a]

[a]Parameter was fixed during refinement.

- Ga^{3+} shows a clear preference for the tetrahedral site compared to the octahedral, while Fe^{3+} is equally distributed between the two.
- The refinement of the occupancy factor for the split O4 position resulted in 0.25(1) with $U = 0.018(2)$ for $Sr_{0.75}Y_{0.25}Co_{0.75}Ga_{0.25}O_{2.625}$ and 0.38(2) with $U = 0.064(6)$ for $Sr_{0.75}Y_{0.25}Co_{0.5}Fe_{0.5}O_{2.625+\delta}$, giving total oxygen stoichiometry $O_{2.63(1)}$ and $O_{2.69(2)}$ for the gallium- and iron-containing substances, respectively. The latter indicates an excess of oxygen at the O4 position. It is physically impossible to locate more than 1/4 oxygen atom at the O4 position, because of too short interatomic distances between neighbouring O4 positions (the longest is 1.47 Å). Therefore, additional oxygen atoms should occupy some other position in the layer, shifted with respect to the O4 position. One may assume that this oxygen position is close to that of the oxygen atoms completing the Co1 polyhedron to form an octahedron (~0.25, 0.5, 0). The assumption of two oxygen positions, at (~0.25, 0.5, 0) and (~0.38, 0.5, 0), was tested and led to decreased reliability factors, from $R_{F^2} = 0.0344$, $\chi^2 = 3.97$, $R_p = 0.0317$ to $R_{F^2} = 0.0274$, $\chi^2 = 3.01$, $R_p = 0.0288$. The refined occupancies of the two positions (~0.38, 0.5, 0) and (~0.25, 0.5, 0) are $g = 0.23(1)$ and 0.15(1) ($U = 0.007(5)$),

respectively. Because of the high correlation between thermal factors and occupancies of the atomic positions, it was decided to fix the *U*-parameter of these two oxygen positions at a value of 0.020. This procedure did not lead to any significant changes of the *R*-values or occupancies of the oxygen positions. The presence of additional oxygen atoms at (~0.25, 0.5, 0) was also tested for $Sr_{0.75}Y_{0.25}Co_{0.75}Ga_{0.25}O_{2.625}$. In this case, however, the occupancy of the additional oxygen position (~0.25, 0.5, 0) refined to 0.04(2), indicating the absence of a noticeable amount of additional oxygen in the structure.

Additional peaks from an ordered magnetic structure were observed in the neutron powder pattern of $Sr_{0.75}Y_{0.25}Co_{0.5}Fe_{0.5}O_{2.625+\delta}$, as shown in Fig. 3a. The magnetic structure was found to be a G-type antiferromagnetic order, similar to that of the Dy-314 phase [2].

All atomic displacement parameters were modelled isotropically. Attempts to use anisotropic factors did not improve the results of the refinement. Selected interatomic distances in $Sr_{0.75}Y_{0.25}Co_{0.75}Ga_{0.25}O_{2.625}$ and $Sr_{0.75}Y_{0.25}Co_{0.5}Fe_{0.5}O_{2.625+\delta}$ are presented in Table 4. The corresponding interatomic distances in $Sr_{0.7}Y_{0.3}CoO_{2.62}$ [1] are included in Table 4 for comparison.

3.2. Electron diffraction study

As mentioned above, the ED patterns of $Sr_{0.75}Y_{0.25}Co_{0.75}Ga_{0.25}O_{2.625}$ could be indexed with an *I*-centred tetragonal unit cell where $a \approx 2a_p$ and $c \approx 4a_p$ ($a_p \approx 3.9$ Å). An ED pattern aligned along the [100] zone axis is shown in Fig. 4a. The crystallites were single domains, i.e. twinning was not frequently observed. This was also confirmed by the HRTEM studies. A HRTEM micrograph of $Sr_{0.75}Y_{0.25}Co_{0.75}Ga_{0.25}O_{2.625}$ aligned along the [100] zone axis is shown in Fig. 5a. On the other hand, microtwinning was frequently observed in the compounds containing iron, as can be seen in the SAED pattern in Fig. 4b and the HRTEM micrograph in Fig. 5b for $Sr_{0.75}Y_{0.25}Co_{0.5}Fe_{0.5}O_{2.625+\delta}$. The ED pattern can be described as a superposition of two [100] patterns rotated 90° with respect to each other, which can also be observed in fast Fourier transforms (FFT) of the different domains in the HRTEM image in Fig. 5b. Typically, microtwinning in perovskite-related systems such as $Ca_2Mn_{2-x}Fe_xO_{6-\delta}$ [8], $Sr_2Co_{2-x}Al_xO_5$ [9] and $SrFe_{1-x}V_xO_{2.5}$ [10] occurs between domains sharing the same perovskite subcell axis, which is also the case for $Sr_{0.75}Y_{0.25}Co_{0.5}Fe_{0.5}O_{2.625+\delta}$. The different neighbouring domains share the same perovskite subcell zone axis, namely $\langle 100 \rangle_p$ (p-perovskite sub-cell) in the case of the HRTEM image in Fig. 5b. The presence of weak superstructure reflections with perovskite subcell index $G = \pm 1/2\langle 011 \rangle_p$ (marked with a short arrow in Fig. 4b) reveals that some domains are oriented along [001] as well. This finding is further supported by the three microdiffraction patterns oriented along [100], [001] and [010] shown in Fig. 6. One explanation for the widespread twinning in the iron-containing compounds and its absence in the gallium-containing ones could be the relation between the perovskite subcell axes. The mismatch between $c/4$ and $a/2$ (both equal to the perovskite subcell axis, a_p) is very small in the iron-containing compounds, see Table 1. There is thus very little structural strain to overcome when combining the [100] and [001] domains. This strain decreases with increasing Fe content. At $x = 0.75$ the two different perovskite subcell axes approach equality ($c/4 = a/2$), leading to a completely disordered structure, i.e. only a perovskite subcell is observed in the XRD and the ED records. In HRTEM and SAED images recorded

Table 4
Selected interatomic distances (Å) and angles for the compounds $Sr_{0.75}Y_{0.25}Co_{1-x}M_xO_{2.625+\delta}$, M = Ga; $x = 0.25$ and Fe; $x = 0.5$

Distances (/Å)		M = Ga	M = Fe	$Sr_{0.7}Y_{0.3}CoO_{2.62}$
Octahedron				
Co2/*M*2–O1	(×4)	1.9205(2)	1.9283(3)	1.9130(1)
Co2/*M*2–O2	(×2)	2.093(2)	2.058(3)	2.084(5)
Tetrahedron/5-coordinated polyhedron				
Co1/*M*1–O2	(×2)	1.836(2)	1.859(3)	1.820(5)
Co1/*M*1–O3	(×2)	1.910(2)	1.954(2)	1.944(8)
Co1/*M*1–O4	(×1)	2.211(6)	2.208(7)	2.18(1)
Co1/*M*1–O5	(×1)	—	1.902(3)	—
Sr/Y environment				
Sr1–O1	(×4)	2.588(4)	2.578(6)	2.604(9)
Sr1–O2	(×4)	3.114(2)	3.107(4)	3.099(3)
Sr1–O3	(×4)	2.855(4)	2.884(6)	2.799(9)
Sr2–O1	(×2)	2.545(3)	2.540(4)	2.552(6)
Sr2–O1	(×2)	2.758(3)	2.772(4)	2.768(6)
Sr2–O2	(×4)	2.7493(5)	2.7528(6)	2.736(3)
Sr2–O3	(×2)	2.658(3)	2.655(5)	2.649(7)
Sr2–O5	(×2)	—	2.74(2)	—
Y3–O1	(×4)	2.553(3)	2.588(5)	2.506(7)
Y3–O2	(×4)	2.350(2)	2.365(4)	2.345(4)
Y3–O4	(×1)	2.421(5)	2.377(7)	2.42(1)
Y3–O5	(×1)	—	3.03(3)	—
Angles(/°)				
Octahedron				
O1–Co2–O1	(×2)	87.3(1)	87.8(1)	86.05(2)
	(×2)	92.67(1)	92.2(1)	93.95(2)
O1–Co2–O2	(×2)	93.37(8)	92.8(1)	93.37(8)
	(×2)	86.63(8)	87.2(1)	86.63(8)
Co2–O1–Co2		170.3	169.7(2)	164.4
Tetrahedron/trigonal bipyramid/octahedral				
O2–Co1–O2	(×1)	152.8(2)	157.9(3)	157.1(2)
O3–Co1–O3	(×1)	104.3(3)	102.2(3)	100.8(4)
O2–Co1–O3	(×4)	98.29(7)	96.9(9)	97.3(1)
O2–Co1–O4	(×2)	76.9(2)	79.3(1)	78.9(1)
O3–Co1–O4	(×2)	111.9(2)	114.7(3)	115.1(4)
O2–Co1–O5	(×4)	—	82.7(2)	—
O3–Co1–O5	(×2)	—	177(1)	—
O3–Co1–O5	(×2)	—	80(1)	—

Interatomic distances and angles for $Sr_{0.7}Y_{0.3}CoO_{2.62}$ are given for comparison [1].

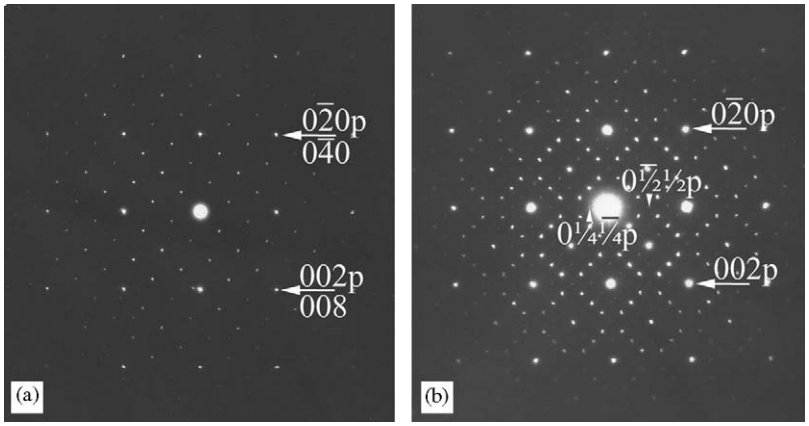

Fig. 4. ED patterns recorded from $Sr_{0.75}Y_{0.25}Co_{0.75}Ga_{0.25}O_{2.625}$ (a) and $Sr_{0.75}Y_{0.25}Co_{0.5}Fe_{0.5}O_{2.625+\delta}$ (b), (a) can be indexed according to the 314 type structure along [100], whereas in (b) microtwinning of differently arranged [100] and [001] zone axis patterns needs to be taken into account along with the breaking of the $I4/mmm$ symmetry discussed in the text.

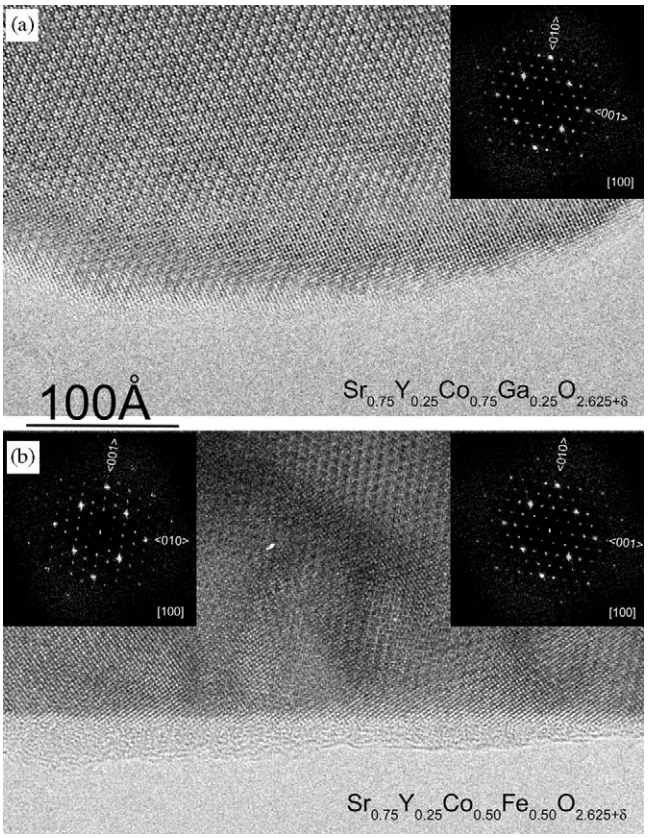

Fig. 5. HRTEM micrographs recorded along [100] for (a) $Sr_{0.75}Y_{0.25}Co_{0.75}Ga_{0.25}O_{2.625}$ and (b) $Sr_{0.75}Y_{0.25}Co_{0.5}Fe_{0.5}O_{2.625+\delta}$. FFTs calculated for the different domains are inserted in the latter micrograph.

from the Fe-substituted compound with $x = 0.75$, only the perovskite substructure is apparent, see Fig. 7.

However, the microtwinning in $Sr_{0.75}Y_{0.25}Co_{0.5}Fe_{0.5}O_{2.625+\delta}$ cannot account for the weak extra reflections at $G = \pm 1/4\langle 011\rangle_p$ (Fig. 4b). This is very similar to what was observed by us [2] and Withers et al. [11] for $Sr_{0.67}Ln_{0.33}CoO_{3-\delta}$ with the 314-type structure. It can be noted that extra reflection were observed only from areas enriched with microdomain boundaries. One explanation could be a local symmetry decrease at the domain boundaries. If the twin plane in the perovskite structure is $\{1\,0\,0\}_p$, then domains aligned along the [100] zone axis will intergrow with domains aligned along [001] and, since $a \neq c/2$, small distortions will occur. In a tetragonal system the angle between $[1\bar{1}0]$ and [110] is 90° by definition, while it differs from 90° between $[0\bar{1}2]$ and [012]. All these directions correspond to the same direction in the perovskite subcell, namely $\langle 110\rangle$. Therefore, to structurally match the two domains, the symmetry must be lowered, which could give rise to superstructure reflections in the ED patterns, like $G \pm 1/4\ \langle 011\rangle_p$ with $d \approx 10.89$ Å. A schematic drawing of such an intergrowth is shown in Fig. 8. Thus the extra reflections could be explained by a monoclinic cell with axes $a \approx b \approx 2\sqrt{2}a_p$ and $\gamma \approx 90°$, as indicated by the bold lines in Fig. 8.

3.3. Magnetic measurements

The temperature dependence of the magnetization is shown in Fig. 9 for $Sr_{0.7}Y_{0.3}CoO_{2.62}$, $Sr_{0.75}Y_{0.25}Co_{0.75}Ga_{0.25}O_{2.625}$ and $Sr_{0.75}Y_{0.25}Co_{0.5}Fe_{0.5}O_{2.625+\delta}$. For all three compounds, a splitting of the ZFC and FC magnetization is observed. The splitting of the magnetization curves can have at least two different origins; either it is due to spontaneous magnetic and electronic phase separation [12], leading to the formation of short-range ordered ferromagnetic clusters embedded in an antiferromagnetically ordered majority phase, or it is due to weak ferromagnetic behaviour caused by a spin-canted antiferromagnetic ground state [13]. The necessary ingredients, in both cases, are the existence of competing antiferromagnetic and ferromagnetic interactions. For $Sr_{0.75}Y_{0.25}Co_{0.5}Fe_{0.5}O_{2.625+\delta}$ the splitting of the ZFC and FC magnetization curves takes place above room temperature, indicating $T_N > T_{room}$, in agreement with the NPD study. The weak splitting could be an indication of a minor spin-canted AFM.

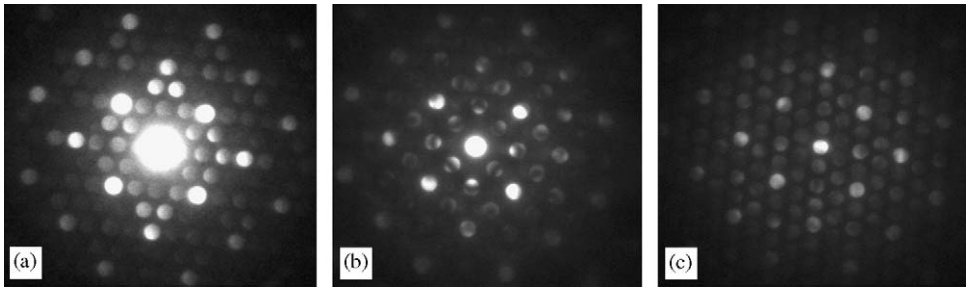

Fig. 6. Electron microdiffraction patterns of $Sr_{0.75}Y_{0.25}Co_{0.5}Fe_{0.5}O_{2.625+\delta}$, taken from the same crystallite along (a) [100], (b) [001] and (c) [100].

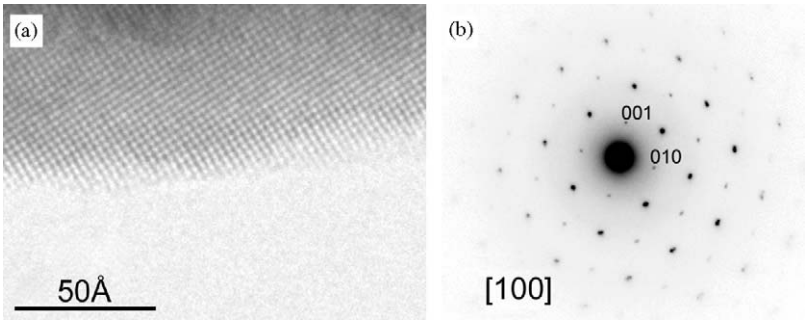

Fig. 7. (a) HRTEM and (b) SAED images recorded from $Sr_{0.75}Y_{0.25}Co_{0.25}Fe_{0.75}O_{2.625+\delta}$. Here, only the perovskite substructure is apparent.

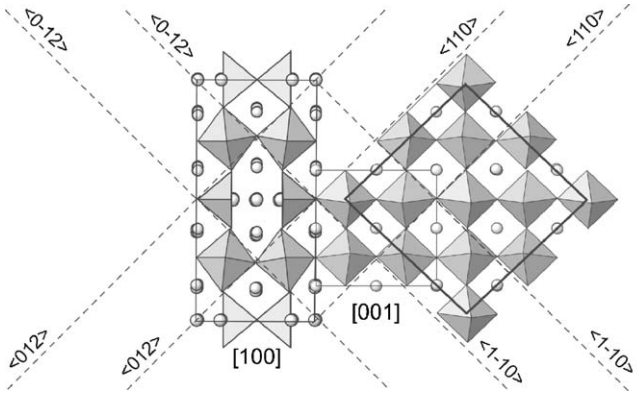

Fig. 8. Model of the boundary between 314 structures oriented along [100] and [001]. At the boundary, the $\langle 012\rangle$ and $\langle 0\bar{1}2\rangle$ axes must have the same direction as $\langle 110\rangle$ and $\langle 1\bar{1}0\rangle$, respectively. The proposed monoclinic cell is indicated by bold lines ($a \approx b \approx 2\sqrt{2}a_p$ and $\gamma \approx 90^\circ$).

The magnetization versus temperature curves for $Sr_{0.7}Y_{0.3}CoO_{2.62}$ and $Sr_{0.75}Y_{0.25}Co_{0.75}Ga_{0.25}O_{2.625}$ reveal that the transitions to the magnetically ordered state occur approximately at 320 and 225 K, respectively, as seen in Fig. 9 (b). A plot of $1/M$ versus temperature (see inset in Fig. 9 (b)) shows a kink at ~350 K, which makes it difficult or at least non-straightforward to extract the transition temperature from such an analysis. Instead, we have used the inflection point in the magnetization versus temperature curves to estimate the magnetic ordering temperature. It should be noted that a similar kink in the $1/M$ versus temperature curve for a $Sr_{0.775}Y_{0.225}CoO_{2.64}$ sample was observed in [14]. Moreover, in [14] it was pointed out that the same kink behaviour was observed for $TbBaCo_2O_{5.5}$ at the orbital-ordering temperature [15]. The splitting of the ZFC and FC curves, for both samples, takes place near the magnetic transition temperature, suggesting that the ordered magnetic state corresponds to a spin-canted antiferromagnetic state, even though an explanation based on magnetic phase separation cannot be ruled out. The dominant antiferromagnetic behaviours of all three samples are supported by the magnetization versus field curves shown in Fig. 10; the magnetization does not saturate even in fields as high as 20 kOe (for $Sr_{0.7}Y_{0.3}CoO_{2.62}$ and $Sr_{0.75}Y_{0.25}Co_{0.75}Ga_{0.25}O_{2.625}$ the field range was extended to 50 kOe). A behaviour similar to that observed here is frequently reported for cobalt oxides with perovskite-related structures, like $Sr_{1-x}Ln_xCoO_{3-\delta}$ [12]. In fact, it has been observed for the unoxidized $Sr_{2/3}Y_{1/3}CoO_{8/3+\delta}$ with 314 structure [5].

The FC magnetization versus temperature curve for $Sr_{0.7}Y_{0.3}CoO_{2.62}$ shows a distinct magnetic transition at 320 K. The weak ZFC magnetization is the result of the comparatively large coercive field ($H_c \approx 1800$ Oe for both temperatures shown in Fig. 10a) in combination with the weak applied field (20 Oe). The transition temperature is close to that reported by Kobayashi et al. [14] for $Sr_{0.75}Y_{0.25}CoO_{3-d}$ ($T_c = 335$ K), but a lower transition temperature ($T_c = 225$ K) has been reported by Maignan et al. [5] for the oxygenated sample $Sr_{0.67}Y_{0.33}CoO_{2.71}$ (corresponding to a Co oxidation number of +3.08). The

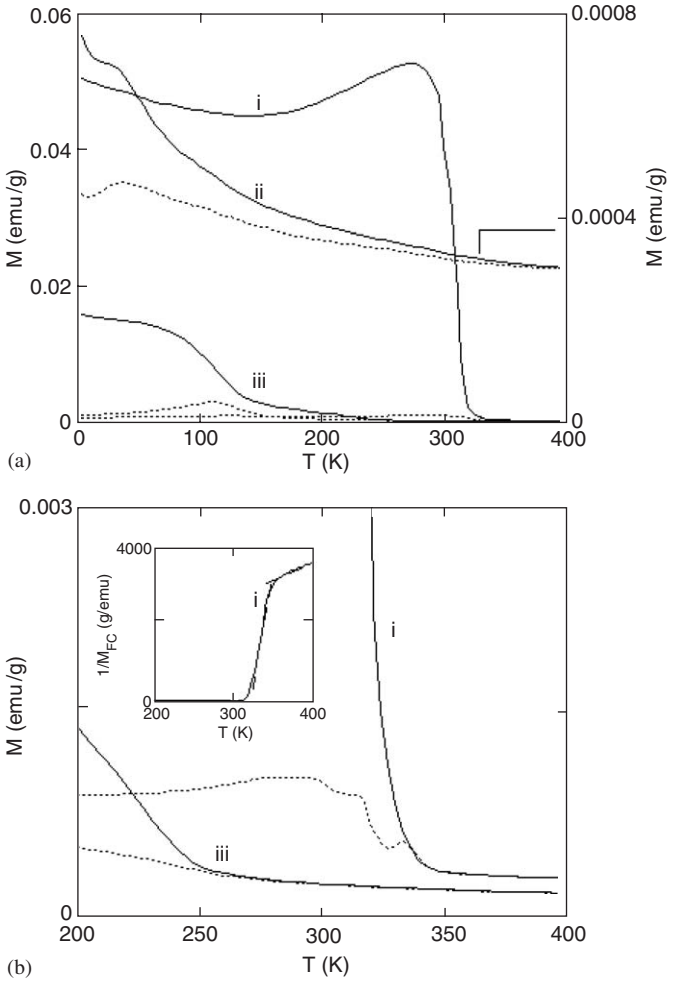

Fig. 9. The temperature dependence of the DC magnetization. Dashed line = ZFC and full line = FC. $Sr_{0.7}Y_{0.3}CoO_{2.62}$ (i), $Sr_{0.75}Y_{0.25}Co_{0.5}Fe_{0.5}O_{2.625+\delta}$ (values at the right), $\delta = 0.076$ (ii) and $Sr_{0.75}Y_{0.25}Co_{0.75}Ga_{0.25}O_{2.625}$ (iii). The figure in (b) is magnified for $Sr_{0.7}Y_{0.3}CoO_{2.62}$ (i) and $Sr_{0.75}Y_{0.25}Co_{0.75}Ga_{0.25}O_{2.625}$ (iii). The inset in (b) shows $1/M_{FC}$ versus temperature for $Sr_{0.7}Y_{0.3}CoO_{2.62}$ (i). $H = 20$ Oe.

NPD patterns of Dy- and Y-314 phases [2,16] all clearly indicate antiferromagnetic ordering of the magnetic moments, irrespective of minor variations in the Y content.

The magnetization versus temperature curves for $Sr_{0.75}Y_{0.25}Co_{0.75}Ga_{0.25}O_{2.625}$ show a magnetic transition at 225 K. Using the simple method suggested in Ref. [12] to separate the ferromagnetic and antiferromagnetic contributions, the high-field magnetization is given by $M_F + \chi_{AF}H$, where M_F is the ferromagnetic contribution, χ_{AF} is the slope of the magnetization versus field curve at high fields, and H is the applied magnetic field. Performing this analysis for the Ga-substituted compound, one finds the rather surprising result that M_F decreases at low enough temperatures (cf. inset in Fig. 10(b)), and that it is largest at the temperature where the FC magnetization versus temperature curve exhibits a strong increase with decreasing temperature. Similar results are found for $Sr_{0.7}Y_{0.3}CoO_{2.62}$.

The magnetization versus temperature curves for $Sr_{0.75}Y_{0.25}Co_{0.5}Fe_{0.5}O_{2.625+\delta}$ show no magnetic transition in the studied temperature range, see Fig. 9a. Considering the antiferromagnetic ordering found in the neutron diffraction study, one may conclude that the temperature range of the magnetization measurements is below the Néel temperature of the iron-substituted compound. The small splitting between the ZFC and FC curves for this compound may indicate the presence of a minor spin canting. The ferromagnetic contribution for the Fe-substituted compound is however much weaker than that of the $Sr_{0.7}Y_{0.3}CoO_{2.62}$ and Ga-substituted compounds.

4. Discussion

Upon the substitution of cobalt in $Sr_{0.75}Y_{0.25}Co_{1-x}Fe_xO_{2.625+\delta}$ it is possible to replace up to 0.875 of Co by Fe. We did not succeed in preparing the Co-free compound $Sr_{0.75}Y_{0.25}FeO_{3-y}$.

In the case of $Sr_{0.75}Y_{0.25}Co_{1-x}Ga_xO_{2.625+\delta}$ it is possible to replace Co by Ga up to $x = 0.375$. The refinement shows that Ga is present in both tetrahedra and octahedra, although with a strong preference for the former position, see Table 3.

An increase in the unit cell volume of the perovskite subcell is observed both for Ga- and Fe-doped compounds, see Fig. 2. The expansion is to be expected, considering the larger ionic radius for six-coordinated Ga^{3+} and Fe^{3+} compared to Co^{3+}: Ga^{3+}(i.r.) = 0.62 Å, Fe^{3+} HS(i.r.) = 0.645 Å, Co^{3+} LS(i.r.) = 0.545 Å and Co^{3+}HS(i.r.) = 0.61 Å [17]. Substitution of iron for cobalt is accompanied by a gradual decrease of the tetragonal distortion of the unit cell, as seen from the variation of the c/a ratio (Table 1). Two linear parts can be clearly seen in Fig. 2 for $Sr_{0.75}Y_{0.25}Co_{1-x}Fe_xO_{2.625+\delta}$, corresponding to the transition to the cubic phase at $x = 0.625$. The increase in the iron content of the 314 phase also leads to an increase in the oxygen content, as revealed by the refinement of the occupancies of the oxygen positions in $Sr_{0.75}Y_{0.25}Co_{0.5}Fe_{0.5}O_{2.625+\delta}$. This result can be explained both by the larger ionic radius of Fe^{3+} in comparison with Co^{3+}, and therefore the higher tendency of Fe^{3+} to increase its coordination number, and by the increased stability of the higher oxidation states of Fe in comparison with Co. The same result was observed for $YBa_2(Fe_{1-x}Co_x)_3O_{8+w}$, where the oxygen content increases with increasing Fe concentration [18]. In the crystal structure of $Sr_{0.75}Y_{0.25}Co_{0.5}Fe_{0.5}O_{2.625+\delta}$, additional oxygen atoms are located in the layers of tetrahedra. Additional oxygen atoms, O5, are located in position (~0.25, 0.5, 0.0) and are thus removed from position (~0.38, 0.5, 0.0), making it possible to increase the amount of oxygen in the layer. One of the possible arrangements of oxygen atoms in the oxygen-deficient layer of $Sr_{0.75}Y_{0.25}Co_{0.5}Fe_{0.5}O_{2.625+\delta}$ is presented in Fig. 11. In this case, the distance between oxygen atoms O4 and O5 is about 2.70 Å, making such arrangement rather probable. One can not exclude the formation of

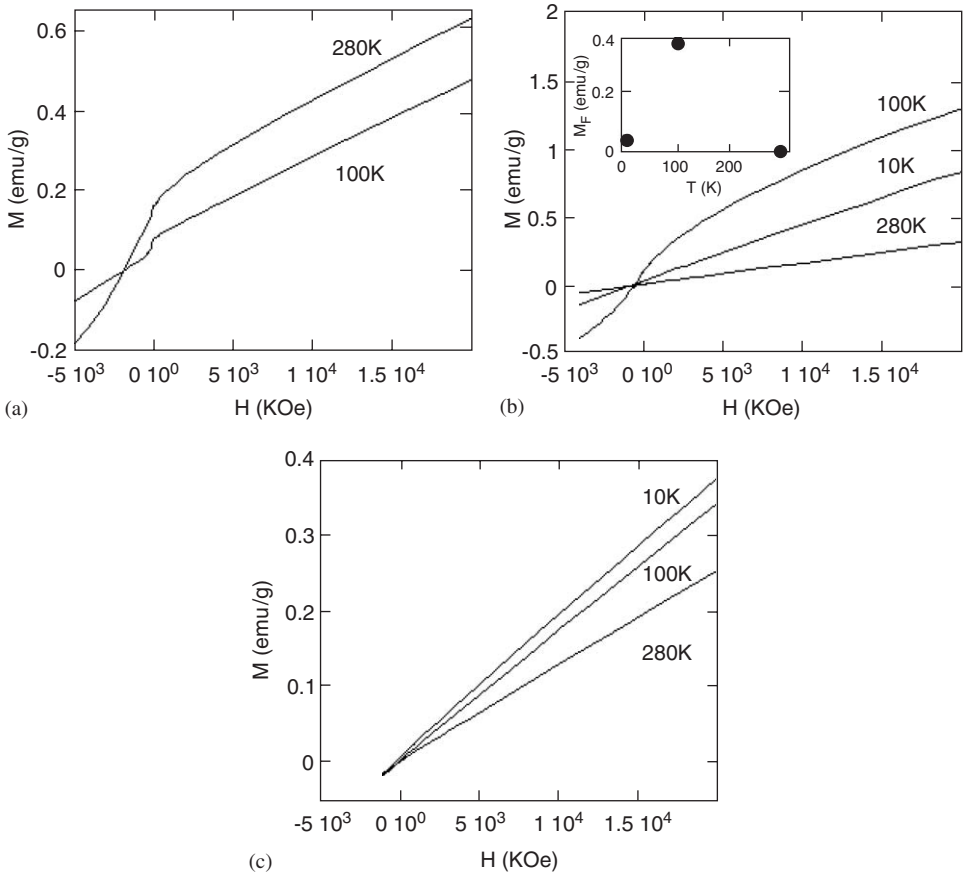

Fig. 10. Magnetisation versus field is shown for samples of $Sr_{0.7}Y_{0.3}CoO_{2.62}$ (a), $Sr_{0.75}Y_{0.25}Co_{0.75}Ga_{0.25}O_{2.625}$ (b) and $Sr_{0.75}Y_{0.25}Co_{0.5}Fe_{0.5}O_{2.625+\delta}$ (c). As discussed in the text, the ferromagnetic contribution to the magnetization of $Sr_{0.7}Y_{0.3}CoO_{2.62}$ and $Sr_{0.75}Y_{0.25}Co_{0.75}Ga_{0.25}O_{2.625}$ decreases at low enough temperatures. The inset in (b) shows M_F versus temperature for $Sr_{0.75}Y_{0.25}Co_{0.75}Ga_{0.25}O_{2.625}$.

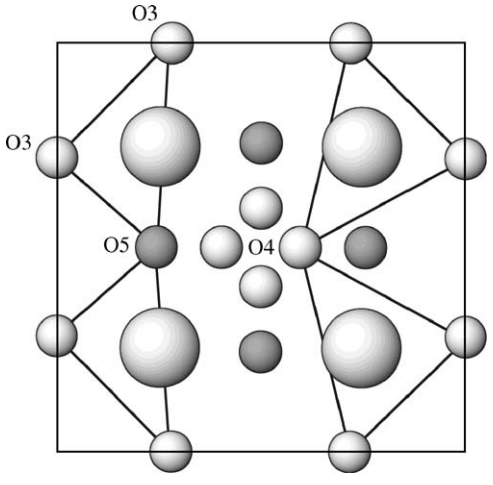

Fig. 11. Distribution of oxygen atoms in the layer of tetrahedra for $Sr_{0.75}Y_{0.25}Co_{0.5}Fe_{0.5}O_{2.625+\delta}$, with the extra oxygen O5 (grey circles) added. One of the possible arrangements of 5-coordinated Co1/Fe1 polyhedra is shown.

octahedra $Co1/Fe1(O2)_2(O5)_4$ in the layer. However, this would lead to the loss of the oxygen O4 from the crystal structure because of too short distances between O4 and O5 (the longest is about 2.10 Å). Our preliminary results from the study of the evolution of the crystal structure of the Dy-314 phase with temperature (500–850 °C) by neutron diffraction shows that O4 oxygen atoms are tightly bonded to rare-earth cations and cannot easily be removed from the crystal structure [19]. Therefore, Co1/Fe1 is most probably only 5-coordinated in the oxygen-deficient layer.

The interatomic distances in $Sr_{0.75}Y_{0.25}Co_{0.75}Ga_{0.25}O_{2.625}$ and $Sr_{0.75}Y_{0.25}Co_{0.5}Fe_{0.5}O_{2.625+\delta}$ are close to those in $Sr_{0.7}Y_{0.3}CoO_{2.62}$, as shown in Table 4. The structures can be described as dilated in the *c* direction compared to the ideal perovskite substructure, leading to one significantly longer *M*2–O2 (axial) distance in the octahedron and a stretched O1–*M*1–O1 angle in the tetrahedron/trigonal bi-pyramid. A similar dilation is also observed in brownmillerites (e.g. in Refs. [20,21]) and is due to the replacement of one layer of octahedra with one of tetrahedra in the process going from ideal perovskite to the oxygen-deficient structure. In the gallium-substituted compound, the *c*-axis remains more or less constant, and the increase of the unit cell volume takes place in the *a*–*b* plane, while in $Sr_{0.75}Y_{0.25}Co_{1-x}Fe_xO_{2.625+\delta}$ all axes increase with increasing *x*. For $Sr_{0.75}Y_{0.25}Co_{0.75}Ga_{0.25}O_{2.625}$ this can be explained by the preference of Ga^{3+} for the tetrahedral position, which leads to a more regular coordination sphere around this position. The tetrahedral angle,

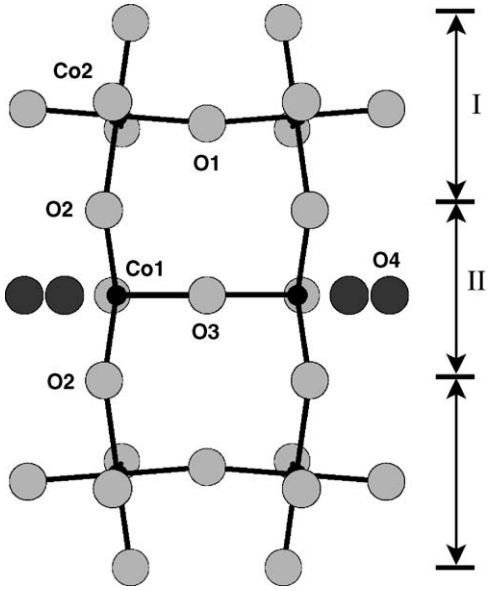

Fig. 12. Crystal structure of the 314 phase, with the *A* cations excluded for clarity. The O2–*M*1–O2 angles for *M*1 are: Co = 157.1°, Co/Ga = 152.8°; Co/Fe = 157.9°. The *M*2–O1–*M*2 angles for *M*2 are: Co = 164.0°, Co/Ga = 170.3°; Co/Fe = 170.8°. The thickness of the slabs of octahedra tetrahedra, I and II respectively, are: for unsubstituted $Sr_{0.7}Y_{0.3}CoO_{2.62}$, I = 4.10 Å, II = 3.60 Å; Fe substituted ($x = 0.5$), I = 4.13 Å, II = 3.65 Å and Ga substituted ($x = 0.25$), I = 4.19 Å, II = 3.57 Å.

O2–*M*1–O2, thus decreases in comparison with $Sr_{0.7}Y_{0.3}CoO_{2.62}$, see Table 4 and Fig. 12. However, the *c*-axis does not shrink since the distortion is counteracted by a small increase of the *M*2–O2 distance and, more important, by decreased puckering of the layers of octahedra. The *M*2–O1–*M*2 angle increases when substituting Co^{3+} for Ga^{3+} (Table 4). For $Sr_{0.75}Y_{0.25}Co_{0.5}Fe_{0.5}O_{2.625+\delta}$ the O2–*M*1–O2 angles in the tetrahedra are very close to that found in the unsubstituted compound, while the apical distance *M*2–O2 in the octahedra is shorter.

Appearance of weak FM in $Sr_{0.7}Y_{0.3}CoO_{2.62}$ was also observed by Kobayashi et al. [14]. The oxygen content of their sample was 2.643(2). The oxygen content of our sample is 2.62(1), as reported in [1], which may explain the small differences in magnetic behaviour observed comparing our sample with that studied in [14]. As shown in [14], the effect of oxygen deficiency is two-fold: the saturation magnetization decreases while the magnetic ordering temperature increases with decreasing oxygen content. Moreover, as shown in [14], the ferromagnetic behaviour of $Sr_{1-x}Y_xCoO_{2.62}$ is most pronounced for yttrium concentrations in the range $0.20 \leqslant x \leqslant 0.25$; the field-induced magnetization for $x = 0.3$ in a field of 1 kOe is approximately 1/10 of that observed for a sample with $x = 0.25$. Magnetic measurements on $Sr_{0.75}Y_{0.25}Co_{0.5}Fe_{0.5}O_{2.625+\delta}$ show that substitution of Co for Fe in the 314 phase leads to suppression of the ferromagnetic-like contribution to the measured magnetization, and values of the magnetic susceptibility are two orders of magnitude less than in undoped $Sr_{0.7}Y_{0.3}CoO_{2.62}$. Moreover, because of the replacement of Co by Fe is accompanied by increasing oxygen content in the 314 phase, it does not lead to the appearance of FM as in the case of an oxygenated 314 phase ($Sr_{2/3}Y_{1/3}CoO_{8/3+\delta}$) [5]. $Sr_{0.75}Y_{0.25}Co_{0.5}Fe_{0.5}O_{2.625+\delta}$ remains antiferromagnetic at room temperature. This result is consistent with the results reported by Kobayashi et al. [14] on Mn-doped Y-314 phase, where even 1% of Mn destroys half of the saturation magnetization.

5. Conclusions

Using a citrate synthesis method, it is possible to replace up to 0.875 of Co by Fe and 0.375 of Co by Ga in $Sr_{0.75}Y_{0.25}Co_{1-x}M_xO_{2.625+\delta}$. Single-phase samples with the 314 structure exist for $M = Ga$, $x \leqslant 0.375$. The 314 structure was found for $Sr_{0.75}Y_{0.25}Co_{1-x}Fe_xO_{2.625+\delta}$, $0.0 \leqslant x \leqslant 0.625$. In the $0.75 \leqslant x \leqslant 0.875$ interval, only the disordered cubic perovskite structure was observed in the XRD pattern.

The structural refinements of $Sr_{0.75}Y_{0.25}Co_{1-x}M_xO_{2.625+\delta}$, $M = Ga$, $x = 0.25$ and $M = Fe$, $x = 0.5$, showed that Ga^{3+} has a preference for the tetrahedral positions while Fe^{3+} is evenly distributed among the tetrahedral and octahedral sites. For $Sr_{0.75}Y_{0.25}Co_{0.5}Fe_{0.5}O_{2.625+\delta}$ the neutron diffraction data could be fitted with a *G*-type antiferromagnetic structure. Replacement of Co by Fe in the Y-314 phase is accompanied by increasing oxygen content, as shown by the refinement of the $Sr_{0.75}Y_{0.25}Co_{0.5}Fe_{0.5}O_{2.625+\delta}$ crystal structure with $\delta = 0.076$.

TEM studies show the gallium-containing 314 compounds to be well ordered, whereas a domain-like intergrowth that gives rise to superstructure reflections in the ED patterns is observed for the iron analogues. The superstructure reflections can be indexed with an orthorhombic or a monoclinic unit cell with $a \approx b \approx 2\sqrt{2}a_p$ and $c \approx 4a_p$ ($\gamma \approx 90°$).

The splitting of the ZFC and FC curves showing the temperature dependence of the magnetization of $Sr_{0.7}Y_{0.3}CoO_{2.62}$ and $Sr_{0.75}Y_{0.25}Co_{0.75}Ga_{0.25}O_{2.625}$ takes place at the magnetic transition temperature, suggesting that the ordered magnetic state corresponds to a spin-canted antiferromagnetic state, although an explanation based on magnetic phase separation cannot be ruled out. Replacing Co by Fe leads to suppression of the ferromagnetic-like contribution to the measured magnetization.

Acknowledgments

This work has been financially supported by the Swedish Research Council (VR) and RFBR (#05-03-32844).

References

[1] S. Ya. Istomin, J. Grins, G. Svensson, O.A. Drozhzhin, V.L. Kozhevnikov, E.V. Antipov, J.P. Attfield, Chem. Mater. 15 (2003) 4012.
[2] S. Ya. Istomin, O.A. Drozhzhin, G. Svensson, E.V. Antipov, Solid State Sci. 6 (2004) 539.
[3] D.K. Smith, Acta Crystallogr. 15 (1962) 1146.

[4] R. Caciuffo, D. Rinaldi, G. Barucca, J. Mira, J. Rivas, M.A. Señarís, P.G. Radaelli, D. Fiorani, J.B. Goodenough, Phys. Rev. B 59 (1999) 1068.
[5] A. Maignan, S. Hébert, V. Caignaert, V. Pralong, D. Pelloquin, J. Solid State Chem. 178 (2005) 868.
[6] A.C. Larson, R.B. Von Dreele, General structure analysis system (GSAS), Los Alamos National Laboratory Report LA-UR-86-748 (2000);
B.H. Toby, EXPGUI, a graphical user interface for GSAS, J. Appl. Crystallogr. 34 (2001) 210.
[7] V.F. Sears, Neutron News 3 (3) (1992) 26.
[8] J.M. González-Calbet, M. Valle-Regí, J. Alsonso, J. Rodríguez-Carvajal, J. Fontcuberta, J. Solid State Chem. 81 (1989) 1.
[9] F. Lindberg, G. Svensson, S.Y. Istomin, S.V. Aleshinskaya, E. Antipov, J. Solid State Chem. 177 (2004) 1592.
[10] N. Nakayama, M. Takano, S. Inamura, N. Nakanishi, K. Kosuge, J. Solid State Chem. 71 (1987) 403.
[11] R.L. Withers, M. James, D.J. Goossens, J. Solid State Chem. 174 (2003) 198.
[12] J. Wu, C. Leighton, Phys. Rev. B 67 (2003) 174408.
[13] P.-G. De Gennes, Phys. Rev. 118 (1960) 141.
[14] W. Kobayashi, S. Ishiwata, I. Terasaki, M. Takano, Phys. Rev. B 72 (2005) 104408.
[15] Y. Moritomo, T. Akimoto, M. Takeo, A. Machida, E. Nishibori, M. Takata, M. Sakata, K. Ohoyama, A. Nakamura, Phys. Rev. B 61 (2000) R13325.
[16] D.J. Goossens, K.F. Wilson, M. James, A.-J. Studer, X.L. Wang, Phys. Rev. B 69 (2004) 134411.
[17] R.D. Shannon, Acta Crystallogr. A 32 (1976) 751.
[18] Q.Z. Huang, V.L. Karen, A. Santoro, A. Kjekshus, J. Linden, T. Pietari, P. Karen, J. Solid State Chem. 172 (2003) 73.
[19] A. Leonidov, S.Y. Istomin, M.V. Patrakeev, A.M. Abakumov, O.A. Drozhzhin, G. Svensson, E.V.Antipov, V.L. Kozhevnikov, to be published elsewhere.
[20] F. Lindberg, S.Ya. Istomin, P. Berastegui, G. Svensson, Kazakov, E.V. Antipov, J. Solid State Chem. 173 (2003) 395.
[21] A.M. Abakumov, M.G. Rozova, B.Ph. Pavlyuk, M.V. Lobanov, E.V. Antipov, O.I. Lebedev, G. van Tendeloo, O.L. Ignatchik, E.A. Ovtchenkov, Yu.A. Koksharov, A.N. Vasilév, J. Solid State Chem. 160 (2001) 353.